An Integrated Approach to Surface Modeling in Freehand Three-Dimensional Echocardiography

Mingzhou Song[1], Robert M. Haralick[2], Florence H. Sheehan[3] and Richard K. Johnson[4]

[1] Department of Computer Science, Queens College, City University of New York, Flushing, NY 11367, USA

[2] Doctoral Program in Computer Science, Graduate Center, City University of New York, New York, NY 10016, USA

[3] Department of Medicine, University of Washington, Seattle, WA 98195, USA

[4] Quantigraphics Inc., P.O. Box 329, Mercer Island, WA 98040, USA

Abstract—We describe an integrated Bayesian solution to find a left ventricle model, including both epicardium and endocardium surfaces, from freehand 3-D echocardiographic images. The observed images and prior shape knowledge are combined to make the most consistent inference about unknown surface models using the maximum *à posteriori* rule. Typical model-based computer vision techniques divide the overall problem into two separate low- and high-level subproblems. Unlike previous approaches, our approach unifies these two levels through a pixel class prediction mechanism. A putative surface model is generated from a catalog of 86 representative surface models. For each observed pixel, its appearance probability profile from different classes is first computed. Then the class predication probability profile is also computed, based only on the putative surface model. An optimal surface model has the best overall match between these two profiles for all the pixels. The probability models are obtained off-line by the expectation maximization algorithm from 20 training studies. Quantitative experimental results on 25 test studies show the advantage of the integrated approach.

I. Introduction

Typical model-based computer vision techniques divide the overall problem into two separate low- and high-level subproblems. In the low level, edge detection or image segmentation is performed. In the high level, geometric models are fit to the features detected from the low level. This paradigm has proven insufficient when the image quality is too poor to reliably detect accurate features.

Echocardiography data are sparse and very noisy, making boundary detection and segmentation of the left ventricle (LV) very difficult in isolated images. We process a set of images in 3D space to determine the surfaces of the LV. Prior shape knowledge must be considered in order to obtain an accurate surface representation. In the integrated framework, the observed images and the prior shape knowledge are combined to make the most consistent inference about unknown surface models using the maximum *à posteriori* rule. As far as we have found in the literature, only Mignotte and Meunier [1] have explored the idea of doing shape modeling from images without an explicit feature detection stage.

Local smoothness is used in [2], [3]. Global parametric shape models have been employed in [4], [5], [6], [7], [8] to enhance the role of shape knowledge. Statistical shape models capture both shape complexity and variations. Cootes *et al* [9] first suggest the 2-D active shape model. Blake and Isard [10] design the 2-D active contour models.

II. Methodology

The integrated approach seeks a solution that is optimal in the sense of maximizing the posterior probability $p(\Theta|Z)$. A putative surface model Θ is generated from a catalog of representative surface models [11]. For each pixel, its appearance probability profile $p(Z|Y)$ from different classes Y is first computed, based on the observed pixel feature vector Z. Then the class predication probability profile $P(Y|\Theta)$ is computed, based only on the putative surface model Θ. An optimal surface model has the best overall match between these two profiles for all the pixels, i.e.,

$$p(\Theta|Z) = \frac{p(\Theta)}{p(Z)} \sum_y p(Z|Y=y)P(Y=y|\Theta) \qquad (1)$$

where $p(\Theta)$ represents the prior shape knowledge. We use a uniform distribution within the convex hull of a catalog of 86 representative LV models. Feature vector Z includes local pixel brightness and directional derivatives. Eq. (1) is true under the assumption that Z and Θ are conditionally independent given class label Y. For the pixel appearance probability model $p(Z|Y)$, the statistically effective and computationally efficient non-parametric optimal quantization [12] representation is employed. For the pixel class prediction probability model $P(Y|\Theta)$, the intensity exponential decaying parametric model is used, in addition to a deterministic imaging simulation process [13].

Off-line training. There are 20 studies in the training set. They have better image quality and complete endocardium (ENDO) and epicardium (EPI) surface models. The goal of training is to obtain the pixel appearance and the pixel class prediction probability models. We estimate them jointly by the expectation maximization algorithm.

Online surface model optimization. We perform an initial alignment of all the members in the LV surface model catalog using three user input landmark points: apex of ENDO, the center of mitral valve and the center of aortic valve, and four user input surface points on ENDO obtained from the short axis view. We apply rotation and translation only to the surface models in the catalog. After the initial alignment, we find a best surface model Θ^*, which is constrained to be a convex combination of members in the aligned catalog, such that $p(\Theta|Z)$ as expressed in Eq. (1) is maximized.

III. Results

We perform the experiment at *end diastole*, when the LV is largest. For every study we select images from standard views – three or four long axis views and one short axis view. The spatial positions and orientations of these images were determined using a magnetic field tracking system. There are 25 test studies, including 6 normal and 19 diseased, neither used in training nor included in the catalog. We measure the projection distance between the optimized and the ground-truth surface models. The ground-truth models are reconstructed from manual delineations. The *projection distance from surface A to surface B* is defined as the mean vertex projection distance from all the vertices of surface A to surface B. The *projection distance between surfaces A and B* is the average of the projection distances from A to B and from B to A. The overall distance errors for ENDO and EPI are 2.6 ± 0.78 mm and 3.2 ± 0.85 mm respectively. The best performance is achieved on the normal group test studies. The diseased studies have various errors.
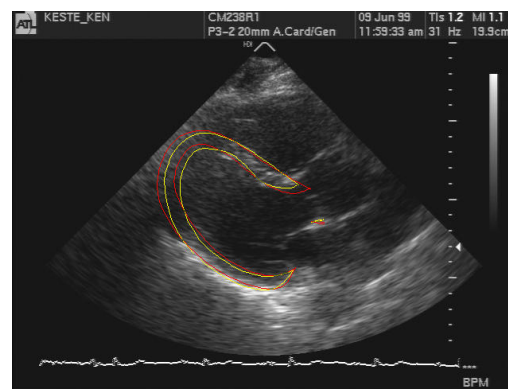
Fig. 1 displays the optimization results on a diseased test study. The figure shows the original images and the imaging plane intersections with the optimized surface models (red) and the ground-truth surface models (yellow). The two surface models agree well at places with strong contrast available, such as the upper and lower center of the view in Fig. 1(a), the lower parts of the view in Fig. 1(c) . However, we observe large error around the area in the upper left of the views in Fig. 1(a) . Image dropout occurs at these places because the local surfaces are almost parallel to the incident ultrasound beam In addition, large errors occurs around the apex area, which is typically either in the near field where distortions are serious or outside the imaging area. Such places will rely more on the the prior shape knowledge and user input points.
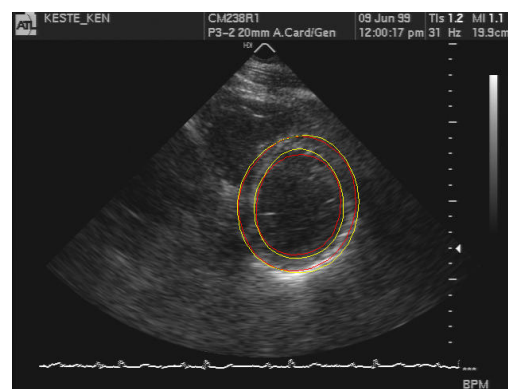
IV. Conclusion

We have presented the integrated approach to LV surface optimization from freehand 3-D echocardiographic images. Our quantitative evaluation has shown this computationally intensive approach performs well on a large number of various normal and diseased clinical studies.
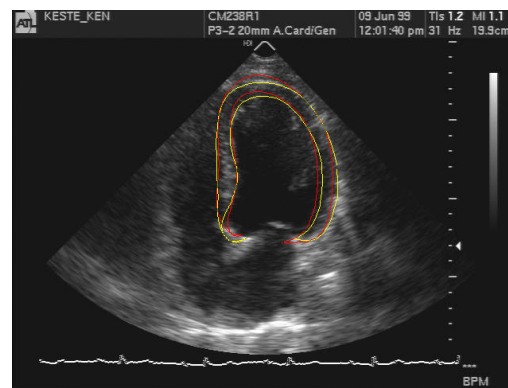
References

[1] M. Mignotte and J. Meunier, "Deformable template and distribution mixture-based data modeling for the encodcarial contour tracking in an echographic sequence," in *Proc. IEEE Comp. Vision and Pattern Recognition*, 1999, pp. 225–30.

[2] M. Kass, A. Witkin, and D. Terzopoulos, "Snakes: active contour models," *Int'l J. of Computer Vision*, vol. 1, no. 4, pp. 321–31, January 1987.

[3] V. Chalana, D. T. Linker, D. R. Haynor, and Y. Kim, "A multiple active contour model for cardiac boundary detection on echocardiographic sequences," *IEEE Trans. Med. Img.*, vol. 15, no. 3, pp. 290–98, June 1996.

[4] E. A. Geiser, D. C. Wilson, D. X. Wang, D. A. Conetta, J. D. Murphy, and A. D. Hutson, "Autonomous epicardial and endocardial boundary detection in echocardiographic short-axis images," *J. of Am. Soc. of Echocardiography*, vol. 11, no. 4, pp. 338–48, April 1998.

[5] James F. Brinkley, "Knowledge-driven ultrasonic three-dimensional organ modeling," *IEEE Trans. PAMI*, vol. 7, no. 4, pp. 431–41, July 1985.

[6] George D. Stetten and Stephen M. Pizer, "Medial-node models to identify and measure objects in real-time 3-D echocardiography," *IEEE Trans. Med. Img.*, vol. 18, no. 10, pp. 1025–34, October 1999.

[7] F. Solina and R. Bajcsy, "Recovery of parametric models from range images: The case for superquadrics with global deformations," *IEEE Trans. PAMI*, vol. 12, no. 2, pp. 131–47, Feb. 1990.

[8] J. Park, D. Metaxas, and L. Axel, "Analysis of left ventricular wall motion based on volumetric deformable models and MRI-SPAMM," *Medical Image Analysis*, vol. 1, no. 1, pp. 53–71, 1996.

[9] T. F. Cootes, A. Hill, C. J. Taylor, and J. Haslam, "The use of active shape models for locating structures in medical images," *Image and Vision Computing*, vol. 12, no. 6, pp. 355–366, July 1994.

[10] A. Blake, B. Bascle, M. Isard, and J. MacCormick, "Statistical models of visual shape and motion," *Phil. Trans. of the Roy. Soc. of London, A*, vol. 356, pp. 1283–1302, 1998.

[11] J. A. McDonald, *Personal Communication*.

[12] M. Song and R. M. Haralick, "Optimal grid quantization," in *Int'l Conf. on Pattern Recognition*, 2002 (in press).

[13] M. Song, R. M. Haralick, and F. H. Sheehan, "Ultrasound imaging simulation and echocardiographic image synthesis," in *Int'l Conf. on Image Processing*, Vancouver, Canada, Sept. 2000.

(a) Parasternal long axis view.

(b) Short axis view.

(c) Apical 4 chamber view.

Fig. 1. A diseased test study. Imaging plane intersections of optimized (red) and true (yellow) surface models.